

---

# PRECL: A new method for interferometry imaging from closure phase

Shiro IKEDA<sup>1,2</sup>, Fumie TAZAKI<sup>3</sup>, Kazunori AKIYAMA<sup>3,4,5</sup>, Kazuhiro HADA<sup>3</sup> & Mareki HONMA<sup>3,6</sup>

<sup>1</sup>The Institute of Statistical Mathematics, Tachikawa, Tokyo, 190-8562, Japan

<sup>2</sup>Department of Statistical Science, Graduate University for Advanced Studies (SOKENDAI), Tachikawa, Tokyo, 190-8562, Japan

<sup>3</sup>Mizusawa VLBI Observatory, National Astronomical Observatory of Japan, Mitaka, Tokyo, 181-8588, Japan

<sup>4</sup>Department of Astronomy, The University of Tokyo, Bunkyo-ku, Tokyo 113-0033, Japan

<sup>5</sup>Massachusetts Institute of Technology, Haystack Observatory, Westford, MA 01886, USA

<sup>6</sup>Department of Astronomical Science, Graduate University for Advanced Studies (SOKENDAI), Mitaka, Tokyo, 181-8588, Japan

\*E-mail: shiro@ism.ac.jp

Received (reception date); Accepted (acceptation date)

## Abstract

For short-wavelength VLBI observations, it is difficult to measure the phase of the visibility function accurately. The closure phases are reliable measurements under this situation, though it is not sufficient to retrieve all of the phase information. We propose a new method, Phase Retrieval from Closure Phase (PRECL). PRECL estimates all the visibility phases only from the closure phases. Combining PRECL with a sparse modeling method we have already proposed, imaging process of VLBI does not rely on dirty image nor self-calibration. The proposed method is tested numerically and the results are promising.

**Key words:** techniques: Interferometric, techniques:image processing, methods: statistics

---

## 1 Introduction

Among observation methods of astronomy, Very Long Baseline Interferometry (VLBI) achieves the highest angular resolution. In particular, VLBI observations at short millimeter wavelength ( $\lesssim 1.3$  mm) achieves unprecedentedly high spatial resolution of few tens of microarcsecond, enabling to image shadows of super-massive black holes in the center of our galaxy Sgr A\* and nearby radio galaxy M87. Although such observations have been technically challenging due to the limited sensitivity of the instruments, fast atmospheric phase fluctuations, and small number of available stations, significant progresses have been made in the last several years with the Event Horizon Telescope (EHT; Doeleman et al. 2008, 2012; Fish et al. 2011; Lu et al. 2012, 2013, 2014; Akiyama et al. 2015).

In interferometry, observations at different stations are in-

tegrated into a complex visibility function, which corresponds to the two-dimensional Fourier transform of the original image. EHT has succeeded in measuring the visibility amplitude (Doeleman et al. 2008, 2012; Fish et al. 2011) and also the phase-related quantity through the closure phases (Lu et al. 2012, 2013; Akiyama et al. 2015; Fish et al. 2016). But it is still difficult to obtain the visibility phases.

The image reconstruction from the visibility function is one of the most important processes in interferometric observations. In particular, high fidelity imaging in super-resolution regime is essential for EHT observations of Sgr A\* and M87, since the expected size of the black hole shadow is comparable to or possibly smaller than the diffraction limit of the telescope. We have proposed a sparse modeling method for super resolution imaging (Honma et al. 2014). The method is robust against

thermal noises and can reconstruct high-fidelity images even in super-resolution regime. However, the method might not be applicable to short-millimeter VLBI data, since the complex information, in other words, phase information of the visibility function is required. In this article, we propose a new method, Phase REtrieval from CLOSure phase (PRECL). PRECL recovers the phase information of visibility function from closure phases (Jennison 1958). Since closure phases are free from station-based phase errors that are dominant in general, PRECL is robust against the measurement errors of the visibility phases due to the fast atmospheric fluctuation or delays in some instruments. Combining PRECL with sparse modeling, an image is reconstructed without any dirty image nor self-calibration (Cornwell & Wilkinson 1981). This idea is similar to BiSpectrum Maximum Entropy Method (BSMEM; Buscher 1994), but PRECL converges quickly by solving a pair of simple optimization problems iteratively. Since the sparse modeling method for imaging is formulated as a convex optimization problem, the whole imaging process of the interferometry will be formulated as a combination of tractable simple optimization problems. We tested the proposed method with two types of simulated data and the results are promising.

The rest of the paper is organized as follows. In Section 2, the problem is mathematically formulated and the details of PRECL are shown. We show the results of numerical experiments in Section 3 and conclude the paper after some discussions in Section 4.

## 2 Phase retrieval from closure phase

In this section, we show the mathematical formulation of the problem and propose PRECL.

### 2.1 Closure phase

The goal of radio interferometric imaging is to reconstruct the brightness distribution  $I(x, y)$  of a target radio source at a wavelength  $\lambda$ , where  $(x, y)$  is a sky coordinate (in the equatorial coordinate system) relative to the reference position so-called the ‘‘phase-tracking center.’’ The observed quantity  $V(u, v)$  is a complex function called visibility, which is related to  $I(x, y)$  by the two-dimensional Fourier transform defined as

$$V(u, v) = \int I(x, y) e^{-2\pi i(ux+vy)} dx dy. \quad (1)$$

Here, the spatial frequency  $(u, v)$  corresponds to the normalized (with  $\lambda$ ) baseline vector between two antennas projected to the tangent plane of the celestial sphere at the phase-tracking center. Since  $I(x, y)$  is real,  $V(u, v)$  has the Hermitian symmetry, that is,  $V(-u, -v) = V^*(u, v)$  where  $*$  denotes the complex conjugate. The visibility is computed as the cross correlation of the input signals at two stations. Thus, the number of the observed

points in  $(u, v)$ -plane is limited by the number of the antennas operating at the same time.

Let  $j$  be the index of measurements where the total number is  $N$ : Corresponding position in  $(u, v)$ -plane is  $(u_j, v_j)$ , recording time is  $t_j$ , and complex visibility function is  $V_j$ . Let us define  $V_j$  with its phase  $\phi_j$  as follows

$$V(u_j, v_j) = V_j = |V_j| e^{i\phi_j}, \quad (2)$$

where, each phase satisfies  $\phi_j \in (-\pi, \pi]$ . In practical situations, instrumental delays and the atmospheric turbulence mostly from the troposphere induce the antenna-based error in the visibility phase. As the result, the observed phase  $\tilde{\phi}_j$  is offset from the true phase  $\phi_j$ . This is a serious problem especially in VLBI observations performed at different sites with non-synchronized local oscillators.

The closure phase is defined as a combination of three different visibility phases recorded at the same time and is known to be free from the antenna-based phase errors (Jennison 1958). Let us show the definition of the closure phase,

$$\psi_m = \tilde{\phi}_j + \tilde{\phi}_k - \tilde{\phi}_l = \phi_j + \phi_k - \phi_l,$$

where  $m$  is the index of the closure phase. The closure phase has been used to calibrate the visibility phases in the VLBI observations (Rogers et al. 1974).

Let  $\phi = (\phi_1, \dots, \phi_N)^T$  and  $\psi = (\psi_1, \dots, \psi_M)^T$  be the visibility and the closure phase vector, respectively. The above relation is summarized as a system of linear equations,

$$\psi = A\phi, \quad (3)$$

where  $A$  is a real  $M \times N$  ( $M < N$ ) matrix. The matrix is sparse that each row has only three nonzero ( $-1$  or  $1$ ) components. The closure phase  $\psi$  is computed from a set of measurements.

### 2.2 Outline of PRECL

PRECL is a method to estimate  $\phi$  from  $\psi$ . Since the system of linear equations in eq. (3) is underdetermined, some additional information must be used.

We rely on an assumption that the phase  $\phi_j$  does not behave randomly but changes smoothly in  $(u, v)$ -plane. In other words, when  $(u_j, v_j)$  and  $(u_k, v_k)$  are close to each other,  $\phi_j$  and  $\phi_k$  are expected to be similar. Now, we consider minimizing the following cost function under the constraint in eq. (3)

$$C(\phi, \xi) = \frac{1}{2} \sum_{j \neq k} w_{jk} (\phi_j - \phi_k - \xi_{jk})^2, \quad (4)$$

where the weight  $w_{jk}$  is positive and symmetric ( $w_{jk} = w_{kj}$ ). Each phase  $\phi_j$  is in the interval  $(-\pi, \pi]$  and the variable  $\xi_{ij} \in \{-2\pi, 0, 2\pi\}$  is introduced in order to absorb the periodicity of the distance measure between two phases. Now, PRECL is defined as an optimization problem.

$$\begin{aligned} \min_{\phi, \xi} C(\phi, \xi) \quad \text{subject to} \quad \psi = A\phi, \quad (5) \\ \phi \in (-\pi, \pi]^N, \quad \xi \in \{-2\pi, 0, 2\pi\}^{N \times (N-1)}. \end{aligned}$$

This is the outline of PRECL.

### 2.3 Defining weights

If one particular  $w_{jk}$  is larger than other weights, corresponding  $\phi_j$  and  $\phi_k$  should be close to make the cost function small. Thus, the result of PRECL largely depends on the weights  $\{w_{jk}\}$ . Here we discuss how to define them.

Relying on the assumption of smoothness, we define  $w_{ij}$  with the polar coordinate system. Let us define two variables as follows,

$$r_j = \sqrt{u_j^2 + v_j^2}, \quad |\theta_{jk}| = \arccos \frac{|u_j u_k + v_j v_k|}{r_j r_k}. \quad (6)$$

The weight  $w_{jk}$  is defined with these variables as follows,

$$w_{jk} = \alpha(r_j, r_k) \beta(|\theta_{jk}|). \quad (7)$$

We have tested different types of functions, and the following combination of  $\alpha$  and  $\beta$  works best.

$$\alpha(r_j, r_k) = \exp\left(-\lambda_r \sqrt{|r_j^2 - r_k^2|}\right) \quad (8)$$

$$\beta(|\theta_{jk}|) = \exp\left(-\lambda_\theta \sqrt{|\theta_{jk}|}\right) \quad (9)$$

where  $\lambda_r$  and  $\lambda_\theta$  are two tunable parameters. We also restrict the number of non-zero components. We first initialize  $w_{jk} = 0$  for all  $(j, k)$ , then choose closest  $D$  points from each  $(u_j, v_j)$  and set those  $w_{jk}$  positive according to eq. (7). This process is repeated for all  $j$  and finally  $w_{jk}$  is made symmetric.

### 2.4 Solving the optimization problem

Since  $\phi$  is real and  $\xi$  is discrete, minimization of  $C(\phi, \xi)$  is a mixed integer programming (MIP) problem. MIP problems are difficult in general. Here, we propose a simple algorithm which converges quickly.

**Algorithm** *Optimization algorithm for PRECL*

1. Initialize  $\xi$  and  $\phi$  to a zero vector.
2. Iterate (i) and (ii) alternately until convergence.
  - (i). Fix  $\xi$  and update  $\phi$  by minimizing  $C(\phi, \xi)$  over  $\phi$ .
  - (ii). Fix  $\phi$  and update  $\xi$  by minimizing  $C(\phi, \xi)$  over  $\xi$ .

Each step of the iteration makes  $C(\phi, \xi)$  smaller and PRECL always converges. We explain steps (i) and (ii) in detail. In step (i),  $\xi$  is fixed and  $C(\phi, \xi)$  is minimized. Optimizing  $C(\phi, \xi)$  over  $\phi$  is formulated as a quadratic programming (QP) problem. In order to see this, let us define a matrix  $H$  and a real vector  $\mathbf{f}$ .

$$H = \{h_{jk}\}, \quad h_{jk} = \begin{cases} -w_{jk} & j \neq k \\ \sum_l w_{jl} & j = k \end{cases}, \\ \mathbf{f} = (f_1, \dots, f_N)^T, \quad f_k = \sum_j w_{jk} \xi_{jk},$$

where  $^T$  denotes transpose.  $H$  is a real symmetric matrix and positive semi-definite. The corresponding QP problem for  $\phi$  is defined as follows

$$\min \left[ \frac{1}{2} \phi^T H \phi + \mathbf{f}^T \phi \right], \quad \text{subject to } A\phi = \psi, \phi \in [-\pi, \pi]^N \quad (10)$$

The above constraint of  $\phi$  is different from that in eq. (5). We solve the above QP problem and treat the boundary condition separately if  $\phi_i = -\pi$  for some  $i$ . The cost functions in  $C(\phi, \xi)$  differs from that in eq. (10) by the term which does not include  $\phi$ . Thus, solving eq. (10) is equivalent to minimizing  $C(\phi, \xi)$  over  $\phi$ . There are many solvers for QP problems<sup>1</sup>.

In step (ii),  $\phi$  is fixed and  $C(\phi, \xi)$  is minimized over  $\xi$ . This is easily solved as follows,

$$\xi_{jk} = \begin{cases} 2\pi, & \text{if } \phi_j - \phi_k > \pi \\ 0, & \text{if } -\pi < \phi_j - \phi_k \leq \pi \\ -2\pi, & \text{if } \phi_j - \phi_k \leq -\pi \end{cases}.$$

This is performed quickly. Note that each step of PRECL converges quickly to its optimum and the cost function decreases monotonically through iterations. It may converge to a local minimum, especially if the phase structure is very complicated.

### 2.5 Sparse modeling method for image reconstruction

The complex visibility function  $V(u, v)$  is reconstructed with the phases retrieved by PRECL. Next step is to reconstruct the intensity map  $I(x, y)$ . We have already proposed a super-resolution method for imaging in Honma et al. (2014). We explain the outline of the method and an extension.

Let the reconstructed visibility vector  $\tilde{\mathbf{V}} = (\tilde{V}_1, \dots, \tilde{V}_{2N})^T$  where we treat real and imaginary part separately as real components. Let the intensity map vector  $\mathbf{I} = (I_1, \dots, I_{L^2})^T$ , where the size of the image is  $L \times L$ . Ideally,  $\tilde{\mathbf{V}}$  and  $\mathbf{I}$  have the following linear relation

$$\tilde{\mathbf{V}} = F\mathbf{I}, \quad (11)$$

where  $F \in \mathbb{R}^{2N \times (L^2)}$  is a real Fourier matrix. Since  $2N < (L^2)$  holds in general for VLBI, image reconstruction is an ill-posed problem. Also, the observations include errors. We have proposed to use LASSO (Tibshirani 1996) to solve the problem. In LASSO, the following cost function is minimized,

$$\min \left[ \frac{1}{2} \|\tilde{\mathbf{V}} - F\mathbf{I}\|_{\ell_2}^2 + \lambda_1 \|\mathbf{I}\|_{\ell_1} \right], \quad \text{subject to } \mathbf{I} \geq 0. \quad (12)$$

Here  $\|\cdot\|_{\ell_2}$  and  $\|\cdot\|_{\ell_1}$  are  $L2$  and  $L1$  norm, respectively. Many algorithms have been proposed to solve the problem. We used an iterative algorithm proposed in Beck & Teboulle (2009b).

The above optimization problem works well for sparse celestial objects. For less sparse objects, one possible solution is to add another regularization term. A typical choice is the total-variation term which is defined as,

<sup>1</sup> We used "IBM ILOG CPLEX Optimizer."

$$TV(\mathbf{I}) = \sum_{i=1}^{L-1} \sum_{j=1}^{L-1} \sqrt{(I_{i,j} - I_{i+1,j})^2 + (I_{i,j} - I_{i,j+1})^2} \\ + \sum_{i=1}^{L-1} |I_{i,L} - I_{i+1,L}| + \sum_{j=1}^{L-1} |I_{L,j} - I_{L,j+1}|,$$

where  $I_{i,j}$  is the  $(i,j)$  pixel of the image. Now the extended problem is

$$\min \left[ \frac{1}{2} \|\tilde{\mathbf{V}} - \mathbf{F}\mathbf{I}\|_{\ell_2}^2 + \lambda_1 \|\mathbf{I}\|_{\ell_1} + \lambda_{TV} TV(\mathbf{I}) \right], \quad (13)$$

subject to  $\mathbf{I} \succeq 0$ .

We call this extension LASSO+TV method. For the algorithm to solve this problem, we used a modified algorithm of Beck & Teboulle (2009a).

### 3 Numerical experiments

We applied PRECL to two types of simulated data sets on the radio galaxy M87 that is one of the most ideal sources to study the nature of relativistic jets (e.g. see Hada et al. 2011, 2012, 2013, 2014 for a review) and also to probe the event-horizon-scale structure of the super-massive black hole (BH) (e.g. Doeleman et al. 2012; Akiyama et al. 2015).

#### 3.1 Simulated data at 7mm

The first data set is based on the results of Very Long Baseline Array (VLBA) observations at 7 mm (43 GHz) presented in Hada et al. (2011). Originally, observational data were reduced in the Astronomical Image Processing System (AIPS) software package of National Radio Astronomical Observatory (NRAO) and then imaged in the DIFMAP software package (Shepherd 1997) through the iterative CLEAN and phase/amplitude self-calibrations (see Hada et al. 2011 for details).

We simulated a VLBA observation at 7 mm with all the ten stations in the AIPS task UVCON. To make a simulated visibility data set of M87, we imported the CLEAN model created in the above procedure into the UVCON task. We adopted a total bandwidth of 128 MHz and a typical System Equivalent Flux Density (SEFD) of  $\sim 1000$  Jy to mimic a real VLBA observing condition at 7 mm<sup>2</sup>. The integration time per simulated visibility was set to 150 seconds, assuming the perfect phase coherence within the integration time. A continuous observing run over 10 hours was assumed in this simulation.

In the millimeter VLBI observations, amplitude calibration can be critical because systematic errors on measured baseline flux densities reduce the imaging sensitivity in general. Here, we assumed the errors of flux density calibration were removed in the initial calibration process. This reflects the realistic situation because, at least at 7 mm observations with VLBA, errors

<sup>2</sup> see the status report of VLBA provided in the NRAO's website <https://science.nrao.edu/facilities/vlba>

can be mostly removed with careful calibration strategies.

The simulated observation data were exported to the AIPS UV-FITS format<sup>3</sup> with the AIPS task FITTP and then imported into our software for PRECL. In the software, the closure phases were computed from the visibility phases and the original visibility phases were discarded. Then, the visibility phases were retrieved by PRECL from the visibility amplitude in the UV-FITS file and the computed closure phases. We used LASSO to create the image (Honma et al. 2014) from the original simulated data and the reconstructed data with PRECL.

In the left of Fig. 1, the image of the M87 is reconstructed with LASSO from the full visibility information. The image in the center of Fig. 1 is reconstructed from the closure phases and the amplitude information of the visibility function using PRECL and LASSO. The  $uv$ -coverage of the measurements are shown in the right. The number of the points of the measurements was 11932 and that of the closure phases was 9258.

In order to apply PRECL to this data, we needed to define  $\lambda_r$ ,  $\lambda_\theta$ , and  $D$ . For this problem, we have the phase calculated by self-calibration and we adjusted  $\lambda_r$ ,  $\lambda_\theta$  and  $D$  to make the results of PRECL close to those phases. As the results, the parameters were set to  $\lambda_r = 6.67 \times 10^{-3}$ ,  $\lambda_\theta = 12.0$  and  $D = 200$ . PRECL converges around 260 sec with a desktop computer (Intel core i7 CPU, Windows 10). The parameter  $\lambda_1$  for LASSO is set to 1 for both (left and center) of the Fig. 1.

Let  $\phi^*$  and  $\hat{\phi}$  be the original and the estimated phase vector, respectively. In order to see the difference between  $\phi^*$  and  $\hat{\phi}$ , we computed the following two functions.

$$d_1(\phi^*, \hat{\phi}) = \frac{1}{N} \sum_{i=1}^N \min(|\phi_i^* - \hat{\phi}_i|, 2\pi - |\phi_i^* - \hat{\phi}_i|), \quad (14)$$

$$d_2(\phi^*, \hat{\phi}) = \frac{1}{N} \sum_{i=1}^N \min(|\phi_i^* - \hat{\phi}_i|, 2\pi - |\phi_i^* - \hat{\phi}_i|)^2. \quad (15)$$

In the present example,  $d_1(\phi^*, \hat{\phi}) = .0533[\text{rad}]$  and  $d_2(\phi^*, \hat{\phi}) = .00460[\text{rad}^2]$ . Some of the retrieved phases are shown in Fig. 2. The phases are shown along three  $uv$ -coverage curves. The results show that the phases are retrieved almost perfectly. The performance does not have any frequency dependency.

#### 3.2 Simulated data at 1.3 mm

The second set of numerical experiments are based on physically motivated models proposed for 1.3 mm emission from M87. We simulated observations on the following four models based on different physical assumptions.

The first model is a simple, but qualitatively correct force-free jet model in magnetically dominated regime presented in Broderick & Loeb (2009) and Lu et al. (2014). We adopted a model image presented in Akiyama et al. (2015), which is

<sup>3</sup> see AIPS MEMO #117 <http://www.aips.nrao.edu/aipsmemo.html>

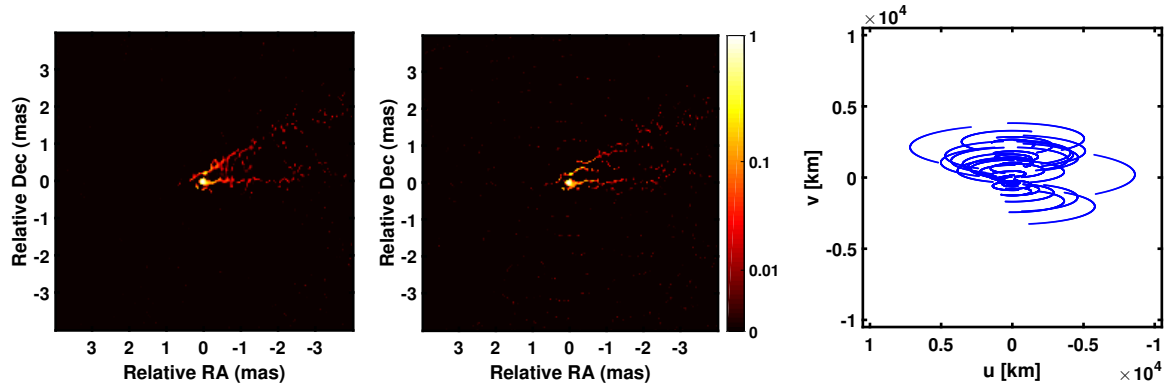


**Fig. 1.** The data sets and the result of the first numerical experiment. The size of each images is  $200 \times 200$  pixels. Intensity is normalized with the maximum value. Left: Image of radio jet in M87 at 43 GHz reconstructed with full information of visibility. Center: Our result. Image of radio jet in M87 at 43 GHz reconstructed from closure phases by PRECL and LASSO. Right:  $uv$ -coverage of the measurement.

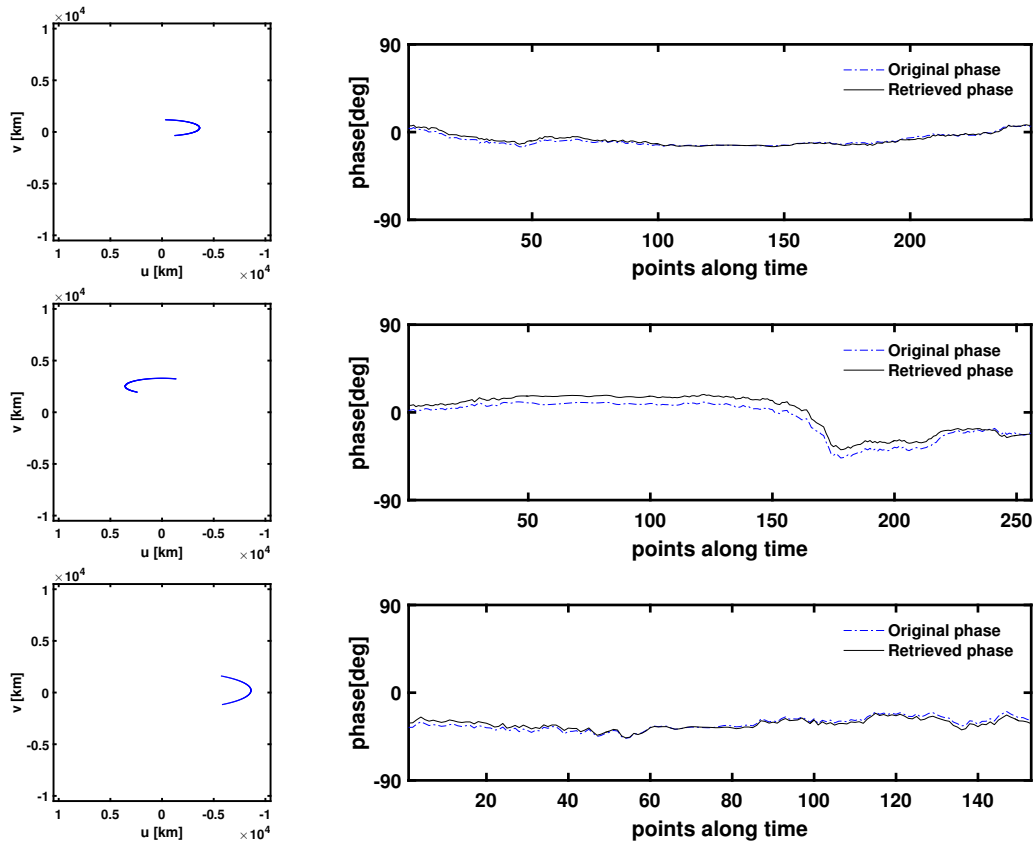


**Fig. 2.** The retrieved phases along the three  $uv$ -coverage curves. Left: A curve corresponds to the  $uv$ -coverage of the station of VLBI. Right: Corresponding phases. Blue half dotted lines show the original phases created by iterative CLEAN and phase/amplitude self-calibration. Black solid lines show the phases retrieved by PRECL.

based on the model parameter fitted to the results of 1.3 mm observations with EHT in Doeleman et al. (2012) and the Spectral Energy Distribution (SED) of M87 (Broderick et al. in preparation). The approaching jet is predominant for this model (see Akiyama et al. 2015) and we call it BL09 (“Broderick & Loeb 2009” model).

The second and third ones are based on results of General

Relativistic Magnetohydrodynamic (GRMHD) simulations presented in Dexter et al. (2012). We use the representative models DJ1 and J2 in Dexter et al. (2012), which are based on the same GRMHD simulation but with different energy and spatial distributions for radio-emitting leptons. The dominant emission region is the accretion disk in DJ1 (“disk + counter jet” model) and the counter jet in J2 (“counter jet” model) illuminating the

last photon orbit. We adopt model images in Akiyama et al. (2015) where the position angle of the large-scale jet for models is adjusted to  $-70^\circ$  inferred for M87 (e.g. Hada et al. 2011).

The last model is based on results of GRMHD simulations presented in Mościbrodzka et al. (2016). We use the image which is time-averaged for  $\sim$  three months for our simulation. The image has a dominant contribution from the counter jet illuminating the last photon orbit similar to J2 of Dexter et al. (2012) but the model assumes energy and spatial distributions of leptons very different to J2. We rotated original images in Mościbrodzka et al. (2016) to adjust the position angle of the large-scale jet to  $-70^\circ$ . We call this model MF15 (“Mościbrodzka & Falcke 2015” model).

The simulated observation data with EHT at 1.3 mm (230 GHz) were generated using the MIT Array Performance Simulator (MAPS) package<sup>4</sup> for each of the above four models. The conditions of simulations followed those in Lu et al. (2014). We adopted a band width of 8 GHz in each of two polarizations which corresponds to a bit rate of 64 Gbit  $s^{-1}$  for four-level signals sampled at the Nyquist rate. This was the target for the Atacama Large Millimeter/submillimeter Array (ALMA) beam former (Fish et al. 2013). We adopted an integration time of 120 s. The simulated observations were performed during 24 hours, and the visibility was sampled at 6 minutes scans with an interval of every 20 minutes when elevations of each station is higher than fifteen degrees.

We assumed perfect phase coherence within the integration time. Typical atmospheric coherence times at 230 GHz are 10 s, but it varies from a few to few tens of seconds depending on the weather condition at each observing site (Doeleman et al. 2009). Although the phase fluctuation due to atmospheric turbulence does not affect the closure phase, such short coherence time can cause serious coherent losses in the coherently-averaged visibility amplitude. However, in practice, the influence of the coherence losses can be removed with established algorithms of the incoherent averaging (Rogers et al. 1995) and indeed have been calibrated in the previous observations (Doeleman et al. 2008, 2012; Fish et al. 2011; Lu et al. 2012, 2013; Akiyama et al. 2015). We assumed the coherence loss on the visibility amplitude was corrected as in the previous observations.

For the other conditions of the simulation, we followed Lu et al. (2014). The array used for the simulation consists of stations at 8 different sites: Hawaii, consisting of one or more of the James Clark Maxwell Telescope (JCMT) and Submillimeter Array (SMA) phased together into a single aperture; the Arizona Radio Observatory Submillimeter Telescope (SMT) on Mount Graham; the Combined Array for Research in Millimeter-wave Astronomy (CARMA) site in California; the Large Millimeter Telescope (LMT) on Sierra Negra, Mexico; the ALMA; the Institut de Radioastronomie Millimétrique

(IRAM) 30 m telescope on Pico Veleta (PV), Spain; the IRAM Plateau de Bure Interferometer (PdBI), phased together as a single aperture; and the Greenland telescope (GLT). The flux density for each station was assumed to be equivalent as in Lu et al. (2014).

Amplitude calibration is critical also at 1.3 mm. Here, we do not include flux density errors as in the case of 7 mm. They were assumed to be removed with existing self-calibration techniques using different types of information, such as, measurements between different bands, polarizations information, and the same sites (Fish et al. 2011; Lu et al. 2012, 2013; Akiyama et al. 2015), and with new techniques using the suitable amplitude calibrator or the closure amplitude information. The problem of these errors will be considered carefully in the future work.

The number of the  $uv$ -coverage points was 1446 while the closure phases were computed for 891 points (Fig. 3.2). The simulated observational data were converted to the AIPS UVFITS format with the MAPS task `maps2uvfits` and then imported into our software for PRECL similarly to the previous 7 mm data. We used LASSO ( $\lambda_1 = 1$ ) to reconstruct images from the original simulated data, where visibility phases were given. For the reconstruction with the phases retrieved by PRECL, we used LASSO+TV ( $\lambda_1 = 15$  and  $\lambda_{TV} = 2$ ). The parameters were set to  $\lambda_r = 5.17 \times 10^{-3}$ ,  $\lambda_\theta = 11.0$ , and  $D = 70$ . The computational time for PRECL was low. It converged with less than 4 iterations of steps (i) and (ii) where the computational time was within 6 sec (Intel core i7 CPU, Windows 10).

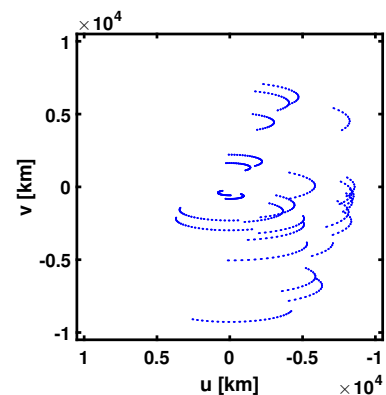
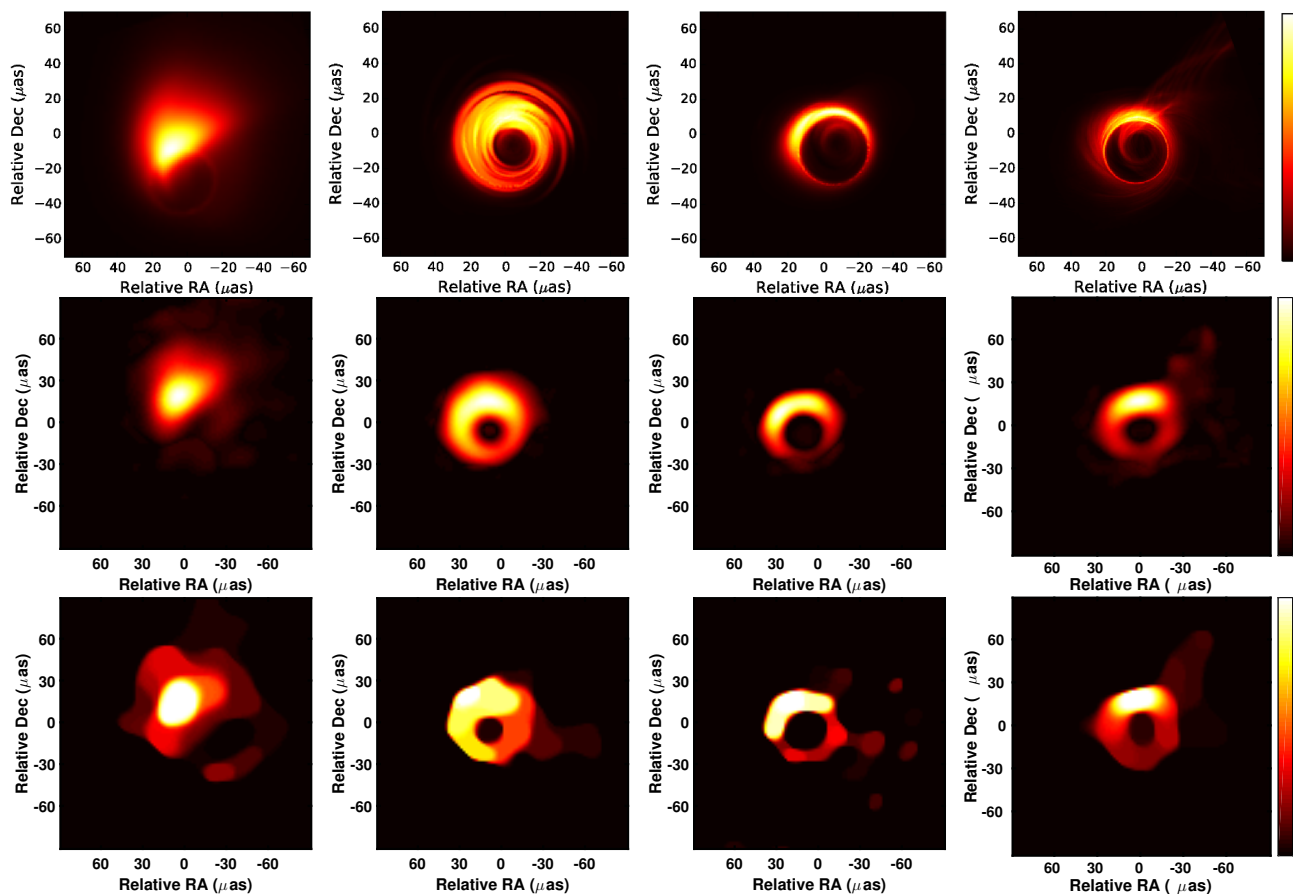


Fig. 3. Simulated EHT  $uv$ -coverage.

The results of PRECL are summarized in Tab. 1. For each model, the cost function of PRECL is calculated with the original phase  $\phi^*$  and the estimated phase  $\hat{\phi}$  and the difference between  $\phi^*$  and  $\hat{\phi}$  is measured with  $d_1(\cdot, \cdot)$  and  $d_2(\cdot, \cdot)$  defined in eqs. (14) and (15), respectively.

The reconstructed images for four models are shown in Fig. 4. The reconstructed images with phase information are compared with the reconstructions only with closure phases. The reconstructions from closure phases are not perfect, but the characteristics of the BH shadows are well preserved.

<sup>4</sup> <http://www.haystack.mit.edu/ast/arrays/maps/>



**Fig. 4.** The reconstructed images. Top row: Original images used for the simulation (Akiyama et al. (2015) (left 3 images) and Mościbrodzka et al. (2016)) Middle row: images reconstructed from full visibility information with LASSO. Image resolutions are  $100 \times 100$  pixels. Bottom row: images reconstructed from closure phases with PRECL and LASSO+TV. Image resolutions are  $100 \times 100$  pixels. From left to right: 1. *BL09* model in Broderick & Loeb (2009) and Lu et al. (2014), 2. *DJ1* model in Dexter et al. (2012), 3. *J2* model in Dexter et al. (2012), and 4. *MF15* model in Mościbrodzka et al. (2016).

**Table 1.** The results of PRECL applied for simulated observations at 1.3 mm:  $\phi^*$  and  $\hat{\phi}$  are the original and the estimated phase, respectively. The cost functions for  $\phi^*$  and  $\hat{\phi}$  are shown in the first and the second row. The difference between  $\phi^*$  and  $\hat{\phi}$  is summarized in the third and the last row with  $d_1(\cdot, \cdot)$  and  $d_2(\cdot, \cdot)$ , respectively.

	BL09	DJ1	J2	MF15
$C(\phi^*, \xi^*)$	1.920	0.890	0.801	0.718
$C(\hat{\phi}, \hat{\xi})$	0.574	0.326	0.262	0.425
$d_1(\phi^*, \hat{\phi})$ [rad]	0.396	0.175	0.204	0.076
$d_2(\phi^*, \hat{\phi})$ [rad <sup>2</sup> ]	0.246	0.053	0.066	0.010

## 4 Discussion

The proposed approach was applied for two types of data. First data set was the simulated 7 mm observation (sec 3.1). In this case, a small and bright celestial object is located in the center, and the phase is rather flat. The retrieved phases are almost

perfect (Fig. 2), and the quality of the reconstructed image is very close to the original image (Fig. 1).

The other data sets were the simulated 1.3 mm observations (sec 3.2). We tested four models. The phase structures are different depending on the model, but all of them have more complicated structures than 7 mm observation because of the BH shadow. The results of PRECL are summarized in Tab. 1. The first and the second row of the table show the values of the cost function. These values reflect the difficulty of the problem. If the phase of the visibility function is not flat but has some structure, the cost function tends to be large. The cost function with the estimated phase is smaller than that with the original phase. This is not surprising since the function was not optimized for the original phase. Although the differences between  $\phi^*$  and  $\hat{\phi}$  are not as small as the 7 mm simulation, they are good enough that the reconstructed images preserve the characteristics of the BH shadows very well (Fig. 4).

In the above numerical experiments, we treated observational/simulated data with relatively small number of stations, i.e., 10 for the VLBA case and 8 for the EHT case. In an ideal

case, the number of independent closure phases for a snap shot observation is given by

$$N_{closure} = \frac{1}{2}(N_{ant} - 1)(N_{ant} - 2), \quad (16)$$

where  $N_{ant}$  is the number of the independent stations. The number of baselines is

$$N_{base} = \frac{1}{2}N_{ant}(N_{ant} - 1). \quad (17)$$

Therefore, the ratio of the closure phases over the baseline phases, which we call ‘‘closure filling factor’’ is given by

$$R_{closure} = \frac{N_{closure}}{N_{base}} = \frac{N_{ant} - 2}{N_{ant}}. \quad (18)$$

Here we assumed that the source is always visible from all the stations. Practically however, some stations could be partially dropped off due to elevation limit depending on the location of the station as well as the source position, and the actual value of  $R_{closure}$  would be somewhat smaller than that for the ideal case. For instance, the EHT simulation above has  $R_{closure} = 891/1446 \sim 0.62$ , while the ideal case for  $N_{ant} = 8$  gives  $R_{closure} = 0.75$ .

If one considers an interferometric array with a larger number of stations, the closure filling factor becomes higher and even close to unity. For instance, in the case of JVLA ( $N_{ant} = 27$ ) the closure filling factor is 0.93, and in the case of ALMA ( $N_{ant} \sim 50$ ) the factor can be as high as 0.96. In these cases,  $R_{closure}$  is nearly unity, and hopefully visibility phases can be retrieved from closure phases with even better accuracy than the results shown above. We note that this would bring a significant impact in calibration and imaging with interferometer: in the interferometric imaging, the key calibration process is that concerning the phase, which is directly affected by the fluctuation of troposphere (and ionosphere as well in case of low frequency observations). Since the closure phase totally cancels out station-based phase fluctuation (both that of troposphere and ionosphere), an introduction of the technique like PRECL can fairly simplify the interferometric calibration process. The trade-off is that if one wants to apply this technique to the interferometry with a large number of stations, it requires large computational costs. This will be an issue for future to be solved by high-speed parallel computing and/or algorithm optimization.

## 5 Summary

We have proposed a new method for phase retrieval. The proposed PRECL is different from the BSMEM (Buscher 1994; Katagiri et al. 1997). The phase retrieval problem is separated from the image reconstruction and solved efficiently with a simple algorithm which always converges. PRECL may converge to a local optimum, but we have not seen any serious problem throughout the numerical experiments in this paper. We will test PRECL with more complicated images to see its general

performance. This is one of our future problems.

We have combined PRECL with sparse modeling methods in order to reconstruct the images. We have tested this combination with simulated data sets. For the simulated BH observations with 7mm, the reconstruction is almost perfect. For 1.3 mm wavelength, the characteristics of the BH shadows are well preserved. Although the quality of the reconstructed images may not be perfect, PRECL is simple, and converges quickly. Therefore, the estimated phases are good enough for the initial values of the phases for iterative CLEAN, or MEM based method.

## Acknowledgment

We would like to thank Drs. A. E. Broderick, J. Dexter and M. Mościbrodzka for providing the data for numerical simulations. We are grateful to the referee, Prof. S. K. Okumura for her constructive suggestions. Finally, we thank the editor, Prof. Tsuboi for his assistance with this submission. This study has been supported by JSPS KAKENHI Grant Number 25120007 and 25120008. KA and KH are supported by a Grant-in-Aid for Research Fellows of the Japan Society for the Promotion of Science (JSPS).

## References

- Akiyama, K., Lu, R.-S., Fish, V. L., et al. 2015, *ApJ*, 870, 150
- Beck, A., & Teboulle, M. 2009a, *IEEE trans. Image Proc.*, 18, 2419
- Beck, A., & Teboulle, M. 2009b, *SIAM J. on Imaging Sci.*, 2, 183
- Broderick, A. E., & Loeb, A. 2009, *ApJ*, 697, 1164
- Buscher, D. 1994, in *Very High Angular Resolution Imaging* (Springer Netherlands), 91–93
- Cornwell, R., & Wilkinson, P. N. 1981, *MNRAS*, 196, 1067
- Dexter, J., McKinney, J. C., & Agol, E. 2012, *MNRAS*, 421, 1517
- Doeleman, S. S., Fish, V. L., Broderick, A. E., Loeb, A., & Rogers, A. E. 2009, *ApJ*, 695, 59
- Doeleman, S. S., Weintroub, J., Rogers, A. E., et al. 2008, *Nature*, 455, 78
- Doeleman, S. S., Fish, V. L., Schenck, D. E., et al. 2012, *Science*, 338, 355
- Fish, V., Alef, W., Anderson, J., et al. 2013, arXiv:1309.3519
- Fish, V. L., Doeleman, S. S., Beaudoin, C., et al. 2011, *ApJL*, 727, L36
- Fish, V. L., et al., 2016, *ApJ*, in press, arXiv:1602.05527
- Hada, K., Doi, A., Kino, M., et al. 2011, *Nature*, 477, 185
- Hada, K., Kino, M., Nagai, H., et al. 2012, *ApJ*, 760, 52
- Hada, K., Kino, M., Doi, A., et al. 2013, *ApJ*, 775, 70
- Hada, K., Giroletti, M., Kino, M., et al. 2014, *ApJ*, 788, 165
- Honma, M., Akiyama, K., Uemura, M., & Ikeda, S. 2014, *PASJ*, 66, 95
- Jennison, R. 1958, *MNRAS*, 118, 276
- Katagiri, S., Morita, K.-I., Kawaguchi, N., & Hayakawa, M. 1997, *PASJ*, 49, 123
- Lu, R.-S., Broderick, A. E., Baron, F., et al. 2014, *ApJ*, 788, 120
- Lu, R.-S., Fish, V. L., Weintroub, J., et al. 2012, *ApJL*, 757, L14
- Lu, R.-S., Fish, V. L., Akiyama, K., et al. 2013, *ApJ*, 772, 13
- Mościbrodzka, M., Falcke, H., & Shikawa, H. 2016, *A&A*, 586, A38



- Rogers, A., Hinteregger, H., Whitney, A., et al. 1974, *ApJ*, 193, 293  
Rogers, A. E., Doeleman, S. S., & Moran, J. M. 1995, *AJ*, 109, 1391  
Shepherd, M. 1997, *G. Hunt & HE Payne* (San Francisco, CA: ASP), 77  
Tibshirani, R. 1996, *J. R. Statist. Soc. B*, 58, 267